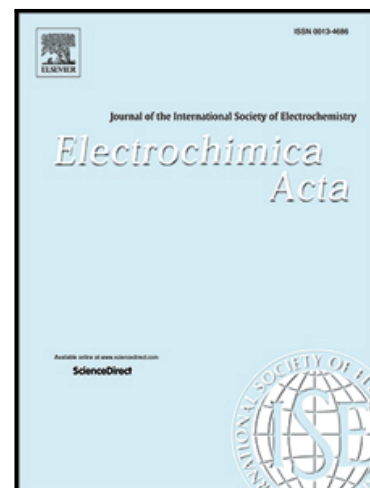


Journal Pre-proof

Electrochemical characterization of alloy segregation in the near-surface deformed layer of welded zones of an Al–Cu–Li alloy using scanning electrochemical microscopy

Rejane Maria P. da Silva , Javier Izquierdo , Mariana X. Milagre , João Victor de S. Araujo , Renato A. Antunes , Ricardo M. Souto , Isolda Costa

PII: S0013-4686(22)01032-5
DOI: <https://doi.org/10.1016/j.electacta.2022.140873>
Reference: EA 140873



To appear in: *Electrochimica Acta*

Received date: 9 March 2022
Revised date: 5 July 2022
Accepted date: 16 July 2022

Please cite this article as: Rejane Maria P. da Silva , Javier Izquierdo , Mariana X. Milagre , João Victor de S. Araujo , Renato A. Antunes , Ricardo M. Souto , Isolda Costa , Electrochemical characterization of alloy segregation in the near-surface deformed layer of welded zones of an Al–Cu–Li alloy using scanning electrochemical microscopy, *Electrochimica Acta* (2022), doi: <https://doi.org/10.1016/j.electacta.2022.140873>

This is a PDF file of an article that has undergone enhancements after acceptance, such as the addition of a cover page and metadata, and formatting for readability, but it is not yet the definitive version of record. This version will undergo additional copyediting, typesetting and review before it is published in its final form, but we are providing this version to give early visibility of the article. Please note that, during the production process, errors may be discovered which could affect the content, and all legal disclaimers that apply to the journal pertain.

© 2022 Published by Elsevier Ltd.

Highlights

- Characterization of the near-surface deformed layer (NSDL) in FSWelded 2098-T351.
- Spatially resolved electrochemical activity in NSDL obtained by potentiometric SECM.
- Mg-enriched bands affect the electrochemical behavior of welded areas.
- The NSDL has an anodic electrochemical behavior with respect to the bulk material.
- Highest activity for Mg²⁺ dissolution observed in the HAZ of the retreating side.

Journal Pre-proof

Electrochemical characterization of alloy segregation in the near-surface deformed layer of welded zones of an Al–Cu–Li alloy using scanning electrochemical microscopy

Rejane Maria P. da Silva^{1*}; Javier Izquierdo^{2,3}; Mariana X. Milagre¹; João Victor de S. Araujo¹; Renato A. Antunes⁴; Ricardo M. Souto^{2,3*}; Isolda Costa^{1*}

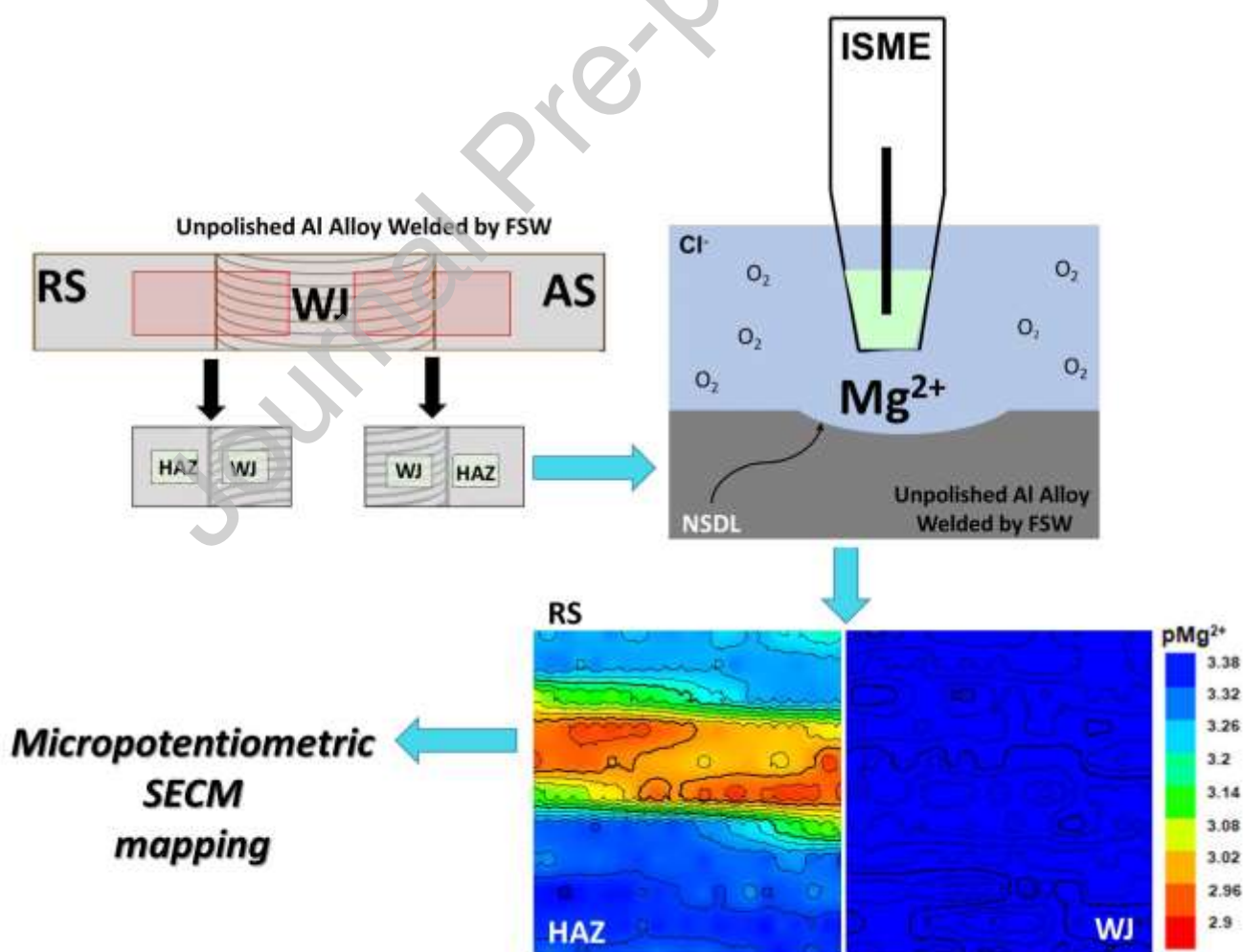
¹ Materials Science and Technology Center, Nuclear and Energy Research Institute – IPEN/CNEN – Av. Prof. Lineu Prestes, 2242, São Paulo, SP, Brazil.

² Department of Chemistry, Universidad de La Laguna, P.O. Box 456, E-38200 La Laguna (Tenerife), Canary Islands, Spain.

³ Institute of Material Science and Nanotechnology, Universidad de La Laguna, P.O. Box 456, E-38200 La Laguna (Tenerife), Canary Islands, Spain.

⁴ Center for Engineering, Modeling and Applied Social Sciences (CECS), Federal University of the ABC (UFABC), Santo André-SP, 09210-580, Brazil.

Graphical abstract



Abstract

The development of heterogeneous electrochemical activity in the welded zones of aluminum alloy 2098-T351 by friction stir welding (FSW) associated with the formation of a near-surface deformed layer (NSDL) upon exposure to an aqueous chloride-containing solution was characterized using scanning electrochemical microscopy (SECM) in potentiometric operation. A solid-contact Mg^{2+} ion-selective microelectrode allowed in situ monitoring of the corrosion reactions sites for magnesium dissolution from different zones of the FSW weld upon exposure to a chloride-containing aqueous environment. In this way, localized corrosion reactions developing in the galvanically coupled joint/heat affected zones (WJ/HAZ) of the weld were detected and imaged with spatial resolution. The most active domains for local Mg^{2+} concentrations were associated with the HAZ of the retreating side (RS), and these corresponded to Mg oxidation from the Mg-enriched oxide bands in NSDL.

Keywords: 2098-T351 Al alloy; Friction stir welding; near-surface deformed layer; localized electrochemical activity; SECM; Mg^{2+} Ion-selective microelectrode.

Corresponding authors:

Rejane Maria P. da Silva, Instituto de Pesquisas Energéticas e Nucleares - IPEN/CNEN - Av. Prof. Lineu Prestes, 2242 - São Paulo -Brazil.
E-mail: rejanep2silva@gmail.com

Isolda Costa, Instituto de Pesquisas Energéticas e Nucleares - IPEN/CNEN - Av. Prof. Lineu Prestes, 2242 - São Paulo -Brazil.
E-mail: icosta@ipen.br

Ricardo M. Souto, Department of Chemistry, Universidad de La Laguna, P.O. Box 456, E-38200 La Laguna, Tenerife, Canary Islands, Spain.
E-mail: rsouto@ull.es; Tel: +34 922 318067.

1. Introduction

During Al alloy manufacturing processes, such as machining, rolling, extrusion, and mechanical grinding, among others, high shear deformation causes severe plastic strain, forming a near-surface deformed layer (NSDL) in the material [1-4]. This deformation layer exhibits different characteristics from the bulk alloy, namely ultrafine grains and the segregation of alloying elements at the grain boundaries. This happens because in the NSDL, hardening precipitates, which may initially be contained in the material, may dissolve into the alloy matrix during machining. Subsequently, alloying elements, such as Mg and Zn, may segregate at the grain boundaries of the newly produced fine grains in the NSDL [2,5,6], exhibiting microstructures different from those of the bulk material [2,7-10]. In addition, the NSDL significantly influences the corrosion behavior of metallic alloys due to high dislocation densities and residual stresses [3,11-14]. As a result, the NSDL is more susceptible to corrosion than bulk material when exposed to an aerated aqueous solution containing chloride ions at ambient temperature and corrodes preferentially over the raw alloy [5,15]. A near-surface deformed layer is also formed during friction stir welding (FSW) [16], a solid-state process employed for Al alloys which leads to the development of different zones in addition to the unaffected base material, i.e. a thermomechanically affected zone (TMAZ) and a stir zone (SZ) constituting the welded joint (WJ), and a heat-affected zone (HAZ) [16-19]. The development of macrogalvanic corrosion processes due to the coupling between weld zones of different microstructure has been shown for the 2198-T851 alloy using the scanning vibrating electrode technique (SVET) and localized electrochemical impedance spectroscopy (LEIS) [20-23]. Although these microelectrochemical methods lacked chemical specificity, i.e. metal dissolution could not be unambiguously attributed to a specific element for a given anodic site, they did help identify sites of cathodic or anodic activity.

Chemically resolved information on local electrochemical activities developed in welded regions should be available using scanning electrochemical microscopy (SECM) with amperometric tips, but they were only able to provide indirect determinations related to oxygen consumption in the cathodic sites or local variations in surface reactivity [17,20,24]. The reason for this situation is the limited applicability of these probes for the characterization

of highly reactive metals that release ionic species with very negative redox potentials (such as aluminum and magnesium) in aqueous environments [25-27]. More recently, a potentiometric probe in combination with a conventional amperometric SECM tip was used to study the electrochemical behavior of coupled FSW weld zones in 2098-T351 Al-Cu-Li [28], as well as its parent material, which has led to the observation that the anodic activity develops preferentially in the HAZ region of the weld. Unfortunately, these studies were performed using the alloy surfaces in a polished state, thus effectively after removal of the NSDL, and therefore did not address the effect of the developed Mg-enriched bands in the NSDL due to metal segregation [15]. Since Mg is a highly reactive metal, it should influence the corrosion activity of as-received alloys with an NSDL. Until now, the specific electrochemical characteristics derived from metal segregation in the alloy have not been obtained.

An alternative procedure to obtain the specific electrochemical activity of a certain metal in an alloy system would be to use an ion-selective microelectrode (ISME) as the tip for the SECM in potentiometric operation [29,30], a procedure already used to monitor metal dissolution from various model galvanic corrosion systems, including cases involving aluminum or magnesium [31-33]. Therefore, this work aims to provide more information on the interfacial and surface chemistry associated with the NSDL in the adjacent zones of the weld joint produced by FSW in the Al-Cu-Li alloy 2098-T351 when exposed to an aqueous NaCl solution using a solid contact Mg^{2+} ion-selective microelectrode (Mg^{2+} -ISME). Although Mg^{2+} -ISME has previously been used to monitor Mg^{2+} ion distributions from pure magnesium or a magnesium alloy exposed to aqueous electrolyte environments [31,32], no designed attempt has been made to detect the small amounts of the metal (~0.3 wt%) present as a minor alloying element in an alloy such as 2098-T351, nor to detect heterogeneous electrochemical activities resulting from the segregation of magnesium during the FSW process. To support the microelectrochemical observations, information on the surface composition in the different weld zones of the alloy was obtained by X-ray Photoelectron Spectroscopy (XPS).

2. Experimental

2.1. Material

The composition in wt% of the 2098-T351 Al-Cu-Li alloy is 3.4 Cu, 1.0 Li, 0.3 Mg, 0.3 Ag, 0.4 Zr, 0.04 Fe, 0.05 Si, 0.02 Zn, 0.003 Mn. The alloy was investigated in the welded condition without grinding or polishing (i.e., the sample material presented the corresponding NDSL). The FSW process was carried out at the Brazilian Nanotechnology National Laboratory (LNNano, Brazilian Center for Research in Energy and Materials, Campinas, SP, Brazil) employing a rotation rate of 1000 rpm and a transverse speed of 150 mm min⁻¹. The diameters of the tool shoulder and the pin were 10 mm and 5 mm, respectively. The surfaces were thoroughly rinsed with deionized water and ethanol before analysis.

2.2. Surface characterization

Scanning electron microscopy (SEM) coupled with Energy Dispersive X-ray Spectroscopy (EDX) using a JEOL JSM-6010LA microscope was employed to reveal the morphology and semi-quantitative composition of the surface of the as-received 2098-T351 Al-Cu-Li alloy in areas of interest, with an analysis depth of approximately 1 µm.

X-ray Photoelectron Spectroscopy (XPS) was used to obtain high resolution Mg2p and O1s spectra of the different weld zones of the alloy produced by the FSW process in order to determine the elemental composition and the possible presence of oxide layers in the first few nanometres of the surface. A Thermo Fisher Scientific K-Alpha+ spectrometer working with a monochromatic Al K-α X-ray source (1486.6 eV), (Waltham, MA, USA) was used. The spot size was 400 µm, the pass energy was 50 eV, and the pressure in the analysis chamber was around 10⁻⁷ Pa. The energy scale was calibrated against the adventitious C1s peak (284.8 eV). Prior to spectra acquisition, the sample surface was cleaned with isopropyl alcohol, followed by conventional cleaning with an argon ions stream at a medium current level for 60 s.

The surfaces of the as received alloy samples retrieved after immersion corrosion tests in a 5 mmol L⁻¹ NaCl solution for periods of exposure to the test solution of up to 16 h at room temperature were characterized using an optical microscope (Leica DMLM; Wetzlar, Germany) coupled to a Leica EC3 camera, controlled by *LASES*[®] software.

2.3. Scanning electrochemical microscopy

The microelectrochemical investigation was performed using a SECM apparatus (Sensolytics, Bochum, Germany), connected to an Autolab electrochemical interface (Metrohm, Herisau, Switzerland). To achieve the potentiometric operation, a 10^{13} input impedance operational amplifier (TL071, Texas Instruments, Dallas, TX, USA) was introduced in the voltage follower clamp of the measuring circuit. The SECM probe was a solid contact Mg^{2+} -ISME, and the fabrication, response time determination, and calibration procedures for this ISME have been described elsewhere [31]. A Nernstian behaviour with a slope -29.2 mV decade⁻¹ and response times between 0.2–0.3 s were determined.

The electrochemical cell included an Ag/AgCl/KCl (sat.) reference electrode in addition to the Mg^{2+} -ISME for the potentiometric operation, while the FSW 2098-T351 Al-Cu-Li alloy was placed at the bottom of the cell with its NSDL facing the electrolytic solution. The latter was left unpolarized in the cell. The ISME was positioned at a fixed height (~ 80 μm) above the surface; the vertical tip-substrate distance was established using the gentle approach procedure with the aid of a video camera television system. The SECM maps were recorded using a scan rate of 50 $\mu\text{m s}^{-1}$ and X-Y increments: 25-50 μm , respectively.

3. Results and discussion

3.1. Surface characterization of the NSDL formed in the weld

The occurrence of Mg- and O-rich bands in the NSDL in the rolling direction for the as-received FSW-welded 2098-T351 Al alloy due to the FSW process is supported by the SEM micrograph and EDX maps shown in Figure 1 (as indicated by the yellow arrows). It has been reported in the literature that Mg enrichment in the NSDL occurs due to outward diffusion of Mg during hot working steps [2,34], and this effect was related to the high temperatures reached in the fabrication process, which favored the migration of Mg to the surface and, consequently, its oxidation. The oxidation process would lead to the formation of MgO and the reduction of amorphous alumina, forming the

oxide layer on the surface [35]. Analogously, alloy segregation and heterogeneous Mg-distribution in FSW-2098-T351 aluminum can be associated with the temperatures reached in the weld. Higher temperatures are reached in the AS (i.e. $>400^{\circ}\text{C}$) compared to the RS ($<400^{\circ}\text{C}$) [36] thus favoring the presence of the NSDL in the latter because the oxidation of Mg is favored at temperatures above 400°C [39]. As the Mg oxidation rate increases, the Mg content tends to decrease. Next, Mg oxidation and diffusion rates at the surface increase with temperature [10,37]. Thus, due to the higher temperatures reached in the AS, the Mg content in this region decreases, as it tends to oxidize and, therefore, the Mg content in the formed oxide bands will be smaller.

Therefore, the different zones developed in the weld region were also characterized by XPS obtaining the high resolution Mg2p and O1s spectra of Figure 2. Although O1s peaks were observed in the four regions considered (see Figures 2b,d), Mg2p peaks were obtained in all cases but the WJ coupled with the HAZ(RS), in which no Mg2p signal was detected (see Figure 2a,c). Furthermore, differences in Mg2p and O1s signals were detected in the HAZ (AS) compared to HAZ(RS) as shown in Figure 2e-f, with higher signals recorded in the HAZ(RS). Therefore, it is in this region that the most Mg-enriched bands appear. Moreover, the Mg2p peaks around 1304 eV are generally attributed to Mg oxide [38,39], and the presence of magnesium oxides in these regions was confirmed by inspecting the O1s spectra shown in Figure 2c-d.

3.2. Spatially-resolved microelectrochemical investigation using the Mg^{2+} -ISME

Changes in the surface of the 2098-T351 alloy associated with a corrosive attack in a 5 mmol L^{-1} NaCl solution were first imaged using optical microscopy at different exposure times. In this way, corrosion propagation related to the Mg-enriched bands (indicated by the yellow arrows in Figure 3) could be noted from a large accumulation of corrosion products in these regions. The corrosion activity in these bands started from the first minutes of immersion and gradually increased with time (cf. Figure 3a).

Potentiometric SECM tests were performed using the Mg^{2+} -ISME to image spatially resolved pMg^{2+} distributions developing in the electrolyte

adjacent to FSW 2098-T351 Al alloy during 2 h immersion in 5 mmol L⁻¹ NaCl solution. The electrochemical activity that develops at each of the coupled WJ/HAZ interfaces formed in the alloy on both the receding side (RS) and on the advancing side (AS) of the welding were determined by exposing them separately to the test electrolyte as shown in Figure 4.

Figure 5 shows the local concentration distributions of Mg²⁺ ions as 2D array scan maps. They evidence a localized corrosion attack with more active domains for Mg²⁺ dissolution in the HAZ zones compared to the WJ zones, and this activity is more intense in the RS. A galvanic coupling mechanism can be associated to the welded zones of friction stir welded 2098-T351 aluminum alloy as received, considering that the Mg-rich bands were removed from the WJ zone during the welding process, and the HAZ is richer in Mg, preferentially on the retreating side. Then, the HAZ is expected to be anodic compared to WJ, while higher Mg dissolution should occur in the HAZ regions. Indeed, the 2D array scan map in Figure 5a, which was obtained in the HAZ(RS) zone, shows the highest concentrations of Mg²⁺ among all the regions, a feature that is particularly notorious when the HAZ(RS) is compared to the HAZ(AS) (see Figure 5c). Furthermore, the shape of the concentration distributions in Figure 5a corresponds to a localized band-like corrosion attack, which must be related to the Mg-enriched bands occurring in this region. Thus, when the Mg²⁺-ISME passes over the Mg-enriched oxide band (NSDL), it detects the Mg²⁺ ions generated by the preferential dissolution of this metal. Since Mg²⁺ formation occurs preferentially in the NSDL and is favored in the HAZ(RS) during welding, the potentiometric SECM map given in Figure 5a showing the HAZ(RS) activity corresponds to the higher Mg content in the oxide bands, and results in the observation of increased electrochemical activity in this region, where the attack is deeper compared to the adjacent regions of the alloy [49]. This result confirms that the underlying bulk material is protected from corrosion due to the cathodic activity sustaining the anodic dissolution of the Mg-enriched band (NSDL), which is more active and therefore dissolves preferentially. This observation was confirmed by the optical micrographs shown in Figure 6 which were made on the samples recovered after performing the SECM measurements. The occurrence of a localized corrosive attack in the form of

bands was observed in the HAZ(RS) region, that is to say in the zone of greatest dissolution of Mg according to SECM (cf. Figure 5).

In summary, the initial stages of corrosion in FSW 2098-T351 alloy is a highly localized electrochemical process that occurs in the near-surface deformed layer as result of alloy segregation during the FSW process. That is, the heterogeneous distribution of Mg along the weld leads to the anodic activation of the heat affected zone of the retreating side (i.e. HAZ(RS)) through a microgalvanic coupling mechanism in the joint/heat affected zones (WJ/HAZ) of the weld where the bulk material is protected against dissolution at this stage. This heterogeneous degradation process in the weld has been imaged *in situ* with chemical resolution for the first time using SECM in potentiometric mode, and has been largely ignored in the scientific literature due to the removal of the NSDL during surface preparation steps such as grinding and polishing, or chemical etching. In this way, the seemingly contradictory results observed in previous studies of this material which showed higher metal dissolution occurring on the advancing side than for RS from SVET maps [28] and when tracking the amount of Al^{3+} species that dissolve from the material [33] in polished samples of FSW 2098-T351. Such an apparent contradiction stems from the failure to detect the impact of magnesium dissolution from the anodic sites that develop in the HAZ(RS) after removal of NSDL during surface preparation.

5. Conclusions

The heterogeneous electrochemical activity across the weld produced on 2098-T351 aluminum alloy by friction stir welding upon exposure to an aqueous electrolyte solution was imaged *in situ* using a solid-contact Mg^{2+} ion-selective microelectrode as probe in the potentiometric operation of the SECM. In this way, a microgalvanic mechanism was observed to account for the localized corrosion process associated with the near-surface deformed layer (NSDL) formed during the welding process.

The electrochemical activities in the coupled WJ/HAZ zones were studied separately. The potentiometric SECM results showed that the NSDL has an anodic electrochemical behavior with respect to the underlying bulk material. Localized corrosion attack occurred in the form of bands like the Mg-enriched

bands that form during the FSW process, and the most active domains for Mg^{2+} dissolution were found in the HAZ (RS) region and exhibited band-like shapes.

High-resolution XPS spectra of the $Mg2p$ and $O1s$ signals obtained from the coupled WJ/HAZ zones, on both RS and AS sides, evidenced that Mg-enriched bands were preferentially found in the HAZ(RS), which was the region of highest electrochemical activity according to SECM measurements. Further observations of preferential corrosive attack in the HAZ(RS) were made by taking optical micrographs of the weld after completing the microelectrochemical and exposure tests in 5 mmol L^{-1} NaCl solution.

The application of ISME potentiometric tips in SECM for the study of the local electrochemical behavior in the welding zones of Al alloys which present a NSDL has been demonstrated in this work and can constitute a significant contribution in the field.

Acknowledgements

The authors acknowledge Fundação de Amparo à Pesquisa do Estado de São Paulo (FAPESP; Proc. 2013/13235-6, Proc.2018/06880-6 and Proc. 2019/11427-1), as well as the University of La Laguna and the Spanish Ministry of Science, Innovation and Universities (Madrid, Spain) under contract No. 2022/0000586, for financial support. The Multiuser Central Facilities (CEM) of UFABC is acknowledged for the experimental support.

References

- [1] G.M. Scamans, M.F. Frolish, W.M. Rainforth, Z. Zhou, Y. Liu, X. Zhou, G.E. Thompson, The ubiquitous Beilby layer on aluminium surfaces, *Surface and Interface Analysis*. 42 (2010) 175–179. doi:10.1002/sia.3204.
- [2] X. Zhou, Y. Liu, G.E. Thompson, G.M. Scamans, P. Skeldon, J.A. Hunter, Near-surface deformed layers on rolled aluminum alloys, *Metallurgical and Materials Transactions A: Physical Metallurgy and Materials Science*. 42 (2011) 1373–1385. doi:10.1007/s11661-010-0538-2.
- [3] Y. Liu, T. Hashimoto, X. Zhou, G.E. Thompson, G.M. Scamans, W.M. Rainforth, J.A. Hunter, Influence of near-surface deformed layers on filiform corrosion of AA3104 aluminium alloy, *Surface and Interface*

- Analysis. 45 (2013) 1553–1557. doi:10.1002/sia.5232.
- [4] J. Wang, X. Zhou, G.E. Thompson, J.A. Hunter, Y. Yuan, Microstructure evolution in the near-surface region during homogenization of a twin-roll cast AlFeMnSi alloy, *Metallurgical and Materials Transactions A: Physical Metallurgy and Materials Science*. 47 (2016) 4268–4275. doi:10.1007/s11661-016-3568-6.
- [5] B. Liu, X. Zhang, X. Zhou, T. Hashimoto, J. Wang, The corrosion behaviour of machined AA7150-T651 aluminium alloy, *Corrosion Science*. 126 (2017) 265–271. doi:10.1016/j.corsci.2017.07.008.
- [6] B. Liu, X. Zhou, T. Hashimoto, X. Zhang, J. Wang, Machining introduced microstructure modification in aluminium alloys, *Journal of Alloys and Compounds*. 757 (2018) 233–238. doi:10.1016/j.jallcom.2018.05.082.
- [7] M.F. Frolich, J.C. Walker, C. Jiao, W.M. Rainforth, J.H. Beynon, Formation and structure of a subsurface layer in hot rolled aluminium alloy AA3104 transfer bar, *Tribology International*. 38 (2005) 1050–1058. doi:10.1016/j.triboint.2005.07.021.
- [8] Y. Liu, M.F. Frolich, W.M. Rainforth, X. Zhou, G.E. Thompson, G.M. Scamans, J.A. Hunter, Evolution of near-surface deformed layers during hot rolling of AA3104 aluminium alloy, *Surface and Interface Analysis*. 42 (2010) 180–184. doi:10.1002/sia.3135.
- [9] J. Wang, X. Zhou, G.E. Thompson, J.A. Hunter, Y. Yuan, Delamination of near-surface layer on cold rolled AlFeSi alloy during sheet forming, *Materials Characterization*. 99 (2015) 109–117. doi:10.1016/j.matchar.2014.11.011.
- [10] J. Wang, X. Zhou, G.E. Thompson, J.A. Hunter, Y. Yuan, Near-surface microstructure on twin-roll cast 8906 aluminum alloy, *Metallurgical and Materials Transactions A*. 46 (2015) 2688–2695. doi:10.1007/s11661-015-2877-5.
- [11] A. Afseth, J.H. Nordlien, G.M. Scamans, K. Nisancioglu, Effect of thermo-mechanical processing on filiform corrosion of aluminium alloy AA3005, *Corrosion Science*. 44 (2002) 2491–2506. doi:10.1016/S0010-938X(02)00036-7.
- [12] X. Zhou, G.E. Thompson, G.M. Scamans, The influence of surface treatment on filiform corrosion resistance of painted aluminium alloy

- sheet, *Corrosion Science*. 45 (2003) 1767–1777. doi:10.1016/S0010-938X(03)00003-9.
- [13] Y. Liu, A. Laurino, T. Hashimoto, X. Zhou, P. Skeldon, G.E. Thompson, G.M. Scamans, C. Blanc, W.M. Rainforth, M.F. Frolish, *Corrosion behaviour of mechanically polished AA7075-T6 aluminium alloy*, *Surface and Interface Analysis*. 42 (2010) 185–188. doi:10.1002/sia.3136.
- [14] J. Seong, F. Yang, F. Scheltens, G.S. Frankel, N. Sridhar, *Influence of the altered surface layer on the corrosion of AA5083*, *Journal of The Electrochemical Society* . 162 (2015) C209–C218. doi:10.1149/2.0321506jes.
- [15] U. Donatus, J.V.S. Araujo, C.S.C. Machado, N.V.V. Mogili, R.A. Antunes, I. Costa, *The effect of manufacturing process induced near-surface deformed layer on the corrosion behaviour of AA2198-T851 Al–Cu–Li alloy*, *Corrosion Engineering, Science and Technology*. 54 (2019) 205–215. doi:10.1080/1478422X.2018.1558932.
- [16] P.L. Threadgill, A.J. Leonard, H.R. Shercliff, P.J. Withers, *Friction stir welding of aluminium alloys*, *International Materials Reviews*. 54 (2009) 49–93. doi:10.1179/174328009X411136.
- [17] U. Donatus, R.M.P. da Silva, J.V.S. Araujo, M.X. Milagre, C.P. de Abreu, C.S.C. Machado, I. Costa, *Macro and microgalvanic interactions in friction stir weldment of AA2198-T851 alloy*, *Journal of Materials Research and Technology*. 8 (2019) 6209–6222. doi:10.1016/j.jmrt.2019.10.015.
- [18] R.W. Fonda, J.F. Bingert, *Precipitation and grain refinement in a 2195 Al friction stir weld*, *Metallurgical and Materials Transactions A: Physical Metallurgy and Materials Science*. 37 (2006) 3593–3604. doi:10.1007/s11661-006-1054-2.
- [19] R. Nandan, T. Debroy, H.K.D.H. Bhadeshia, *Recent Advances in Friction Stir Welding – Process, Weldment Structure and Properties*, *Progress in Materials Science*. 53 (2008) 980–1023. doi:10.1016/j.pmatsci.2008.05.001.
- [20] D. Sidane, E. Bousquet, O. Devos, M. Puiggali, M. Touzet, V. Vivier, A. Poulon-Quintin, *Local electrochemical study of friction stir welded aluminum alloy assembly*, *Journal of Electroanalytical Chemistry*. 737 (2015) 206–211. doi:10.1016/j.jelechem.2014.06.025.

- [21] J.C.B. Bertocello, S.M. Manhabosco, L.F.P. Dick, Corrosion study of the friction stir lap joint of AA7050-T76511 on AA2024-T3 using the scanning vibrating electrode technique, *Corrosion Science*. 94 (2015) 359–367. doi:10.1016/j.corsci.2015.02.029.
- [22] C.P. de Abreu, I. Costa, H.G. de Melo, P. Nadine, B. Tribollet, V. Vivier, Multiscale electrochemical study of welded Al alloys joined by Friction Stir Welding, *Journal of The Electrochemical Society*. 164 (2017) C735-C746. doi:10.1149/2.0391713jes.
- [23] F.M. Queiroz, U. Donatus, O.M.P. Ramirez, J.V.S. Araujo, B.V.G. de Viveiros, S. Lamaka, M. Zheludkevich, M. Masoumi, V. Vivier, I. Costa, H.G. de Melo, Effect of unequal levels of deformation and fragmentation on the electrochemical response of friction stir welded AA2024-T3 alloy, *Electrochimica Acta*. 313 (2019) 271–281. doi:10.1016/j.electacta.2019.04.137.
- [24] M.X. Milagre, U. Donatus, N. V Mogili, R.M.P. Silva, B.V.G. de Viveiros, V.F. Pereira, R.A. Antunes, C.S.C. Machado, J.V.S. Araujo, I. Costa, Galvanic and asymmetry effects on the local electrochemical behavior of the 2098-T351 alloy welded by friction stir welding, *Journal of Materials Science & Technology*. 45 (2020) 162–175. doi:10.1016/j.jmst.2019.11.016.
- [25] A.M. Simões, D. Battocchi, D.E. Tallman, G.P. Bierwagen, SVET and SECM imaging of cathodic protection of aluminium by a Mg-rich coating, *Corrosion Science*. 49 (2007) 3838–3849. doi:10.1016/j.corsci.2007.03.045.
- [26] S.S. Jamali, S.E. Moulton, D.E. Tallman, M. Forsyth, J. Weber, G.G. Wallace, Applications of scanning electrochemical microscopy (SECM) for local characterization of AZ31 surface during corrosion in a buffered media, *Corrosion Science*. 86 (2014) 93–100. doi:10.1016/j.corsci.2014.04.035.
- [27] S. Thomas, J. Izquierdo, N. Birbilis, R.M. Souto, Possibilities and limitations of scanning electrochemical microscopy of Mg and Mg alloys, *Corrosion*. 71 (2015) 171–183. doi:10.5006/1483.
- [28] R.M.P. da Silva, J. Izquierdo, M.X. Milagre, A.M. Betancor-Abreu, L.A. de Oliveira, R.A. Antunes, R.M. Souto, I. Costa, On the local corrosion

- behavior of coupled welded zones of the 2098-T351 Al-Cu-Li alloy produced by Friction Stir Welding (FSW): An amperometric and potentiometric microelectrochemical investigation, *Electrochimica Acta*. 373 (2021) 137910. doi:10.1016/j.electacta.2021.137910.
- [29] B.R. Horrocks, M.V. Mirkin, D.T. Pierce, A.J. Bard, G. Nagy, K. Toth, Scanning electrochemical microscopy. 19. Ion-selective potentiometric microscopy, *Analytical Chemistry*. 65 (1993) 1213–1224. doi:10.1021/ac00057a019.
- [30] G. Nagy, L. Nagy, Electrochemical sensors developed for gathering microscale chemical information, *Analytical Letters*. 40 (2007) 3–38. doi:10.1080/00032710600867226.
- [31] J. Izquierdo, A. Kiss, J.J. Santana, L. Nagy, I. Bitter, H.S. Isaacs, G. Nagy, R.M. Souto, Development of Mg^{2+} ion-selective microelectrodes for potentiometric scanning electrochemical microscopy monitoring of galvanic corrosion processes, *Journal of The Electrochemical Society*. 160 (2013) C451–C459. doi:10.1149/2.001310jes.
- [32] S.H. Salleh, N. Birbilis, M. Musameh, K. Venkatesan, S. Thomas, On the development and application of an in-house fabricated Mg^{2+} ion selective microelectrode (ISME) for assessing Mg corrosion, *Journal of The Electrochemical Society*. 165 (2018) C771-C776. doi:10.1149/2.0591811jes.
- [33] R.M.P. da Silva, J. Izquierdo, M.X. Milagre, R.A. Antunes, R.M. Souto, I. Costa, Development of an Al^{3+} ion-selective microelectrode for the potentiometric microelectrochemical monitoring of corrosion sites on 2098-T351 aluminum alloy surfaces, *Electrochimica Acta*, 415 (2022) 140260. doi: 10.1016/j.electacta.2022.140260.
- [34] K. Shimizu, G.M. Brown, K. Kobayashi, P. Skeldon, G.E. Thompson, G.C. Wood, The early stages of high temperature oxidation of an Al-0.5 wt% Mg alloy, *Corrosion Science*. 40 (1998) 557–575. doi:10.1016/S0010-938X(97)00153-4.
- [35] K. Li, X.R. Zhou, G.E. Thompson, J.A. Hunter, Y.D. Yuan, Evolution of near-surface deformed layers on AA3104 aluminium alloy, *Materials Science Forum*. 765 (2013) 358–362. doi:10.4028/www.scientific.net/MSF.765.358.

- [36] M.X. Milagre, N. V. Mogili, U. Donatus, R.A.R. Giorjão, M. Terada, J.V.S. Araujo, C.S.C. Machado, I. Costa, On the microstructure characterization of the AA2098-T351 alloy welded by FSW, *Materials Characterization*. 140 (2018) 233–246. doi:10.1016/j.matchar.2018.04.015.
- [37] Q. Tan, A. Atrens, N. Mo, M.-X. Zhang, Oxidation of magnesium alloys at elevated temperatures in air: A review, *Corrosion Science*. 112 (2016) 734–759. doi:10.1016/j.corsci.2016.06.018.
- [38] N.C. Haider, J. Alonso, W.E. Swartz, Valence and core electron spectra of Mg in MgO in evaporated thin films, *Zeitschrift Für Naturforschung - Section A Journal of Physical Sciences*. 30 (1975) 1485–1490. doi:10.1515/zna-1975-1119.
- [39] J.E. Qu, M. Ascencio, L.M. Jiang, S. Omanovic, L.X. Yang, Improvement in corrosion resistance of WE43 magnesium alloy by the electrophoretic formation of a ZnO surface coating, *Journal of Coatings Technology and Research*. 16 (2019) 1559–1570. doi:10.1007/s11998-019-00212-7.

Figure captions

Figure 1. SEM image and corresponding EDX distribution maps for Al, Mg and O of the as received 2098-T351 Al alloy.

Figure 2. High resolution Mg2p and O1s spectra measured by XPS in the welding zones of the as received FSW 2098-T351 Al alloy: (a,b) the WJ/HAZ in the retreating side (RS), (c,d) the WJ/HAZ in the advancing side (AS), and (e,f) the HAZ regions (in both RS and AS).

Figure 3. Optical images of the as received 2098-T351 Al alloy after exposure in 5 mmol L⁻¹ NaCl solution for different time periods as indicated. Arrows indicate the NSDL bands.

Figure 4. Sketch of the as received FSW 2098-T351 showing the regions monitored during the microelectrochemical investigation.

Figure 5. Micropotentiometric mapping of local distributions of Mg²⁺ above coupled weldment zones (HAZ/WJ) of the (a,b) retreating side (RS) and (c,d) advancing side (AS) of the as received FSW 2098-T351 Al alloy while freely corroding in 5 mmol L⁻¹ NaCl solution for about 2 h. The SECM maps were obtained using a Mg²⁺-ISME for potentiometric SECM investigation. Tip-substrate distance: 80 μm; scan rate: 50 μm s⁻¹. (pMg = -log₁₀ [Mg²⁺]).

Figure 6. Optical images of the coupled welded zones (HAZ/WJ) of the as received FSW 2098-T351 Al alloy retrieved after completion of SECM testing.

Figure 1

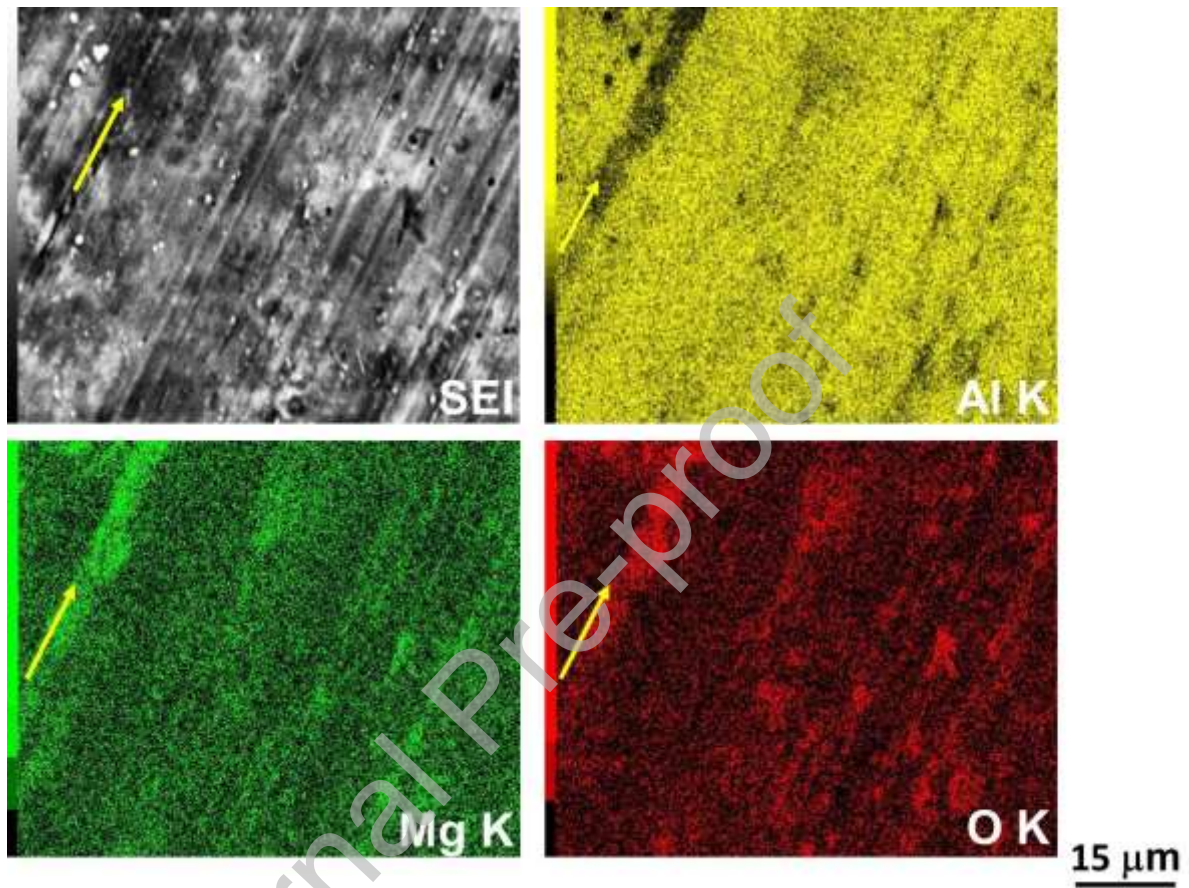


Figure 2

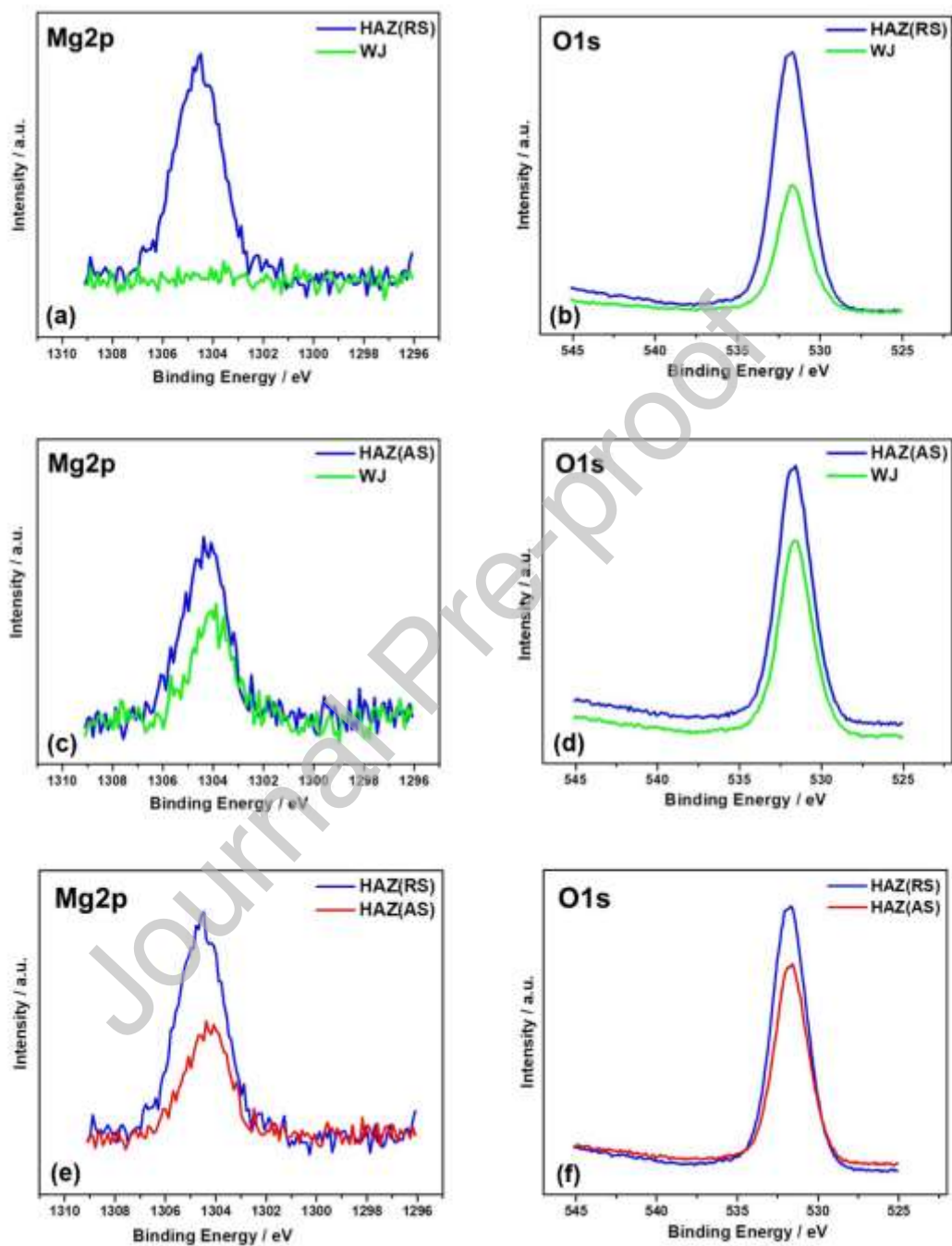


Figure 3

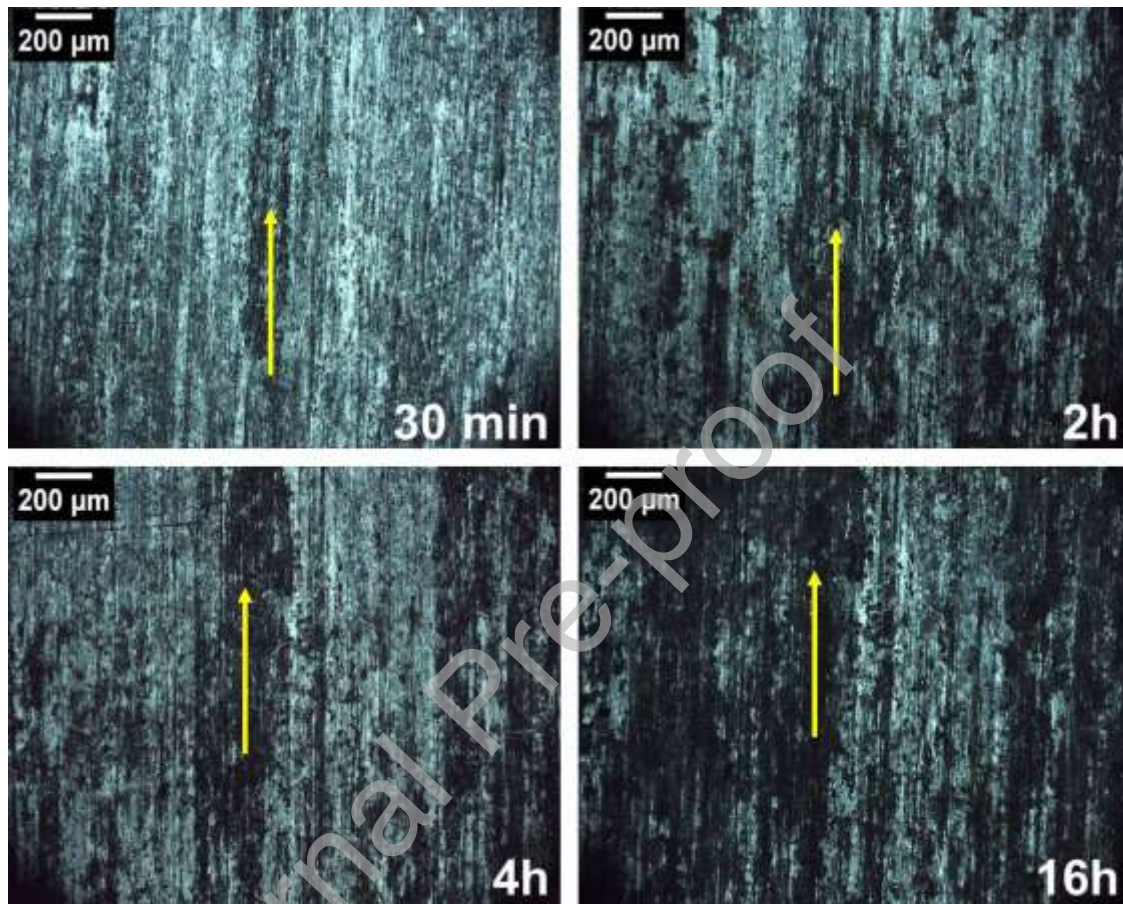


Figure 4

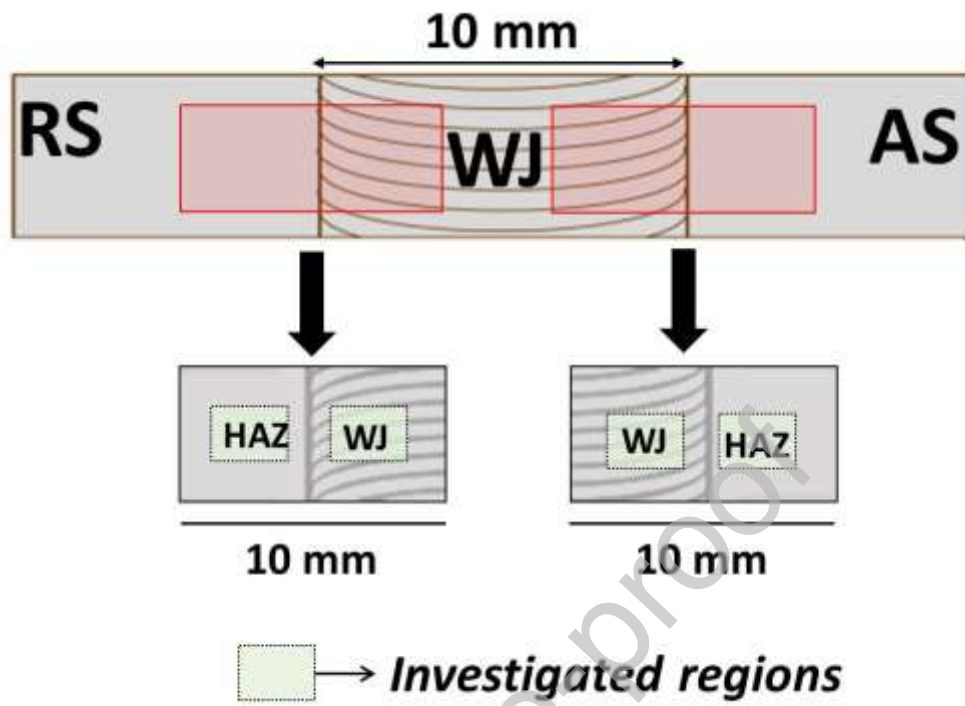


Figure 5

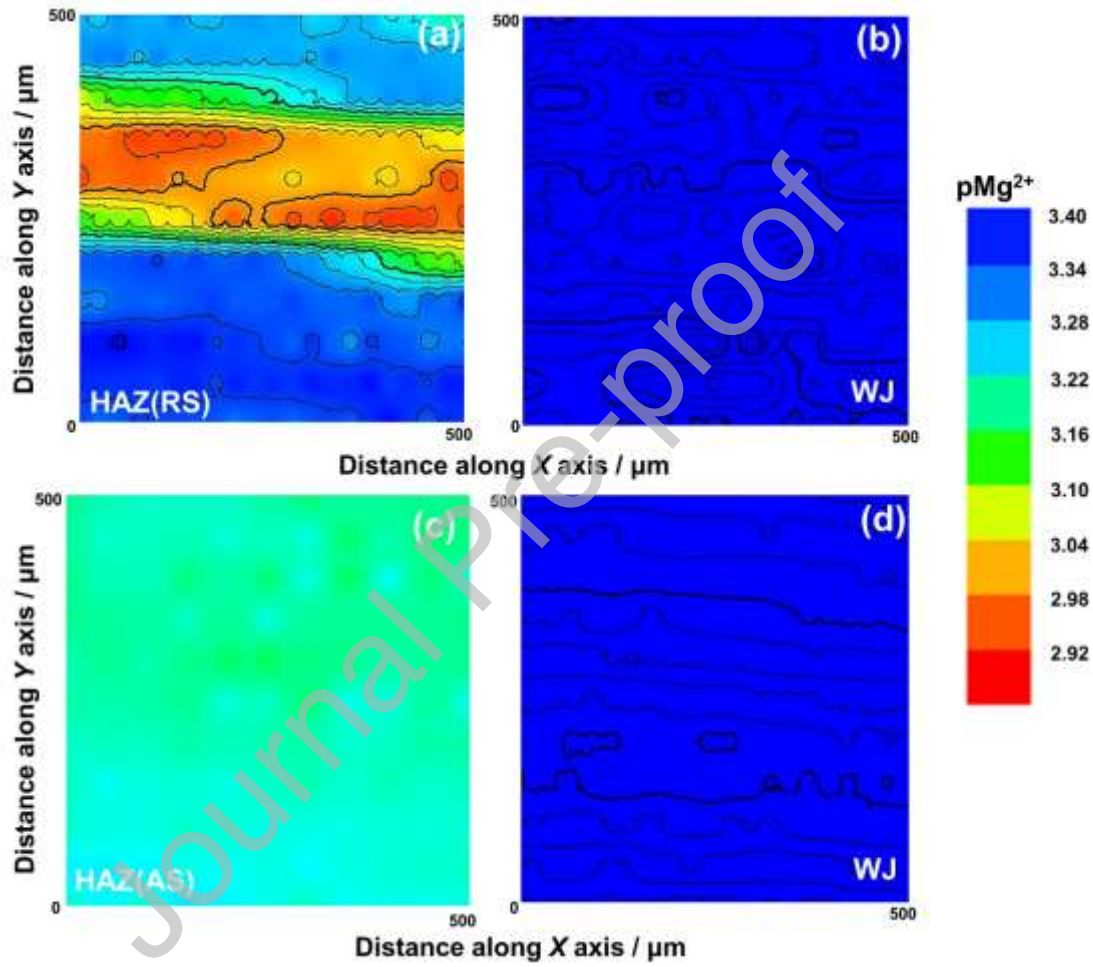
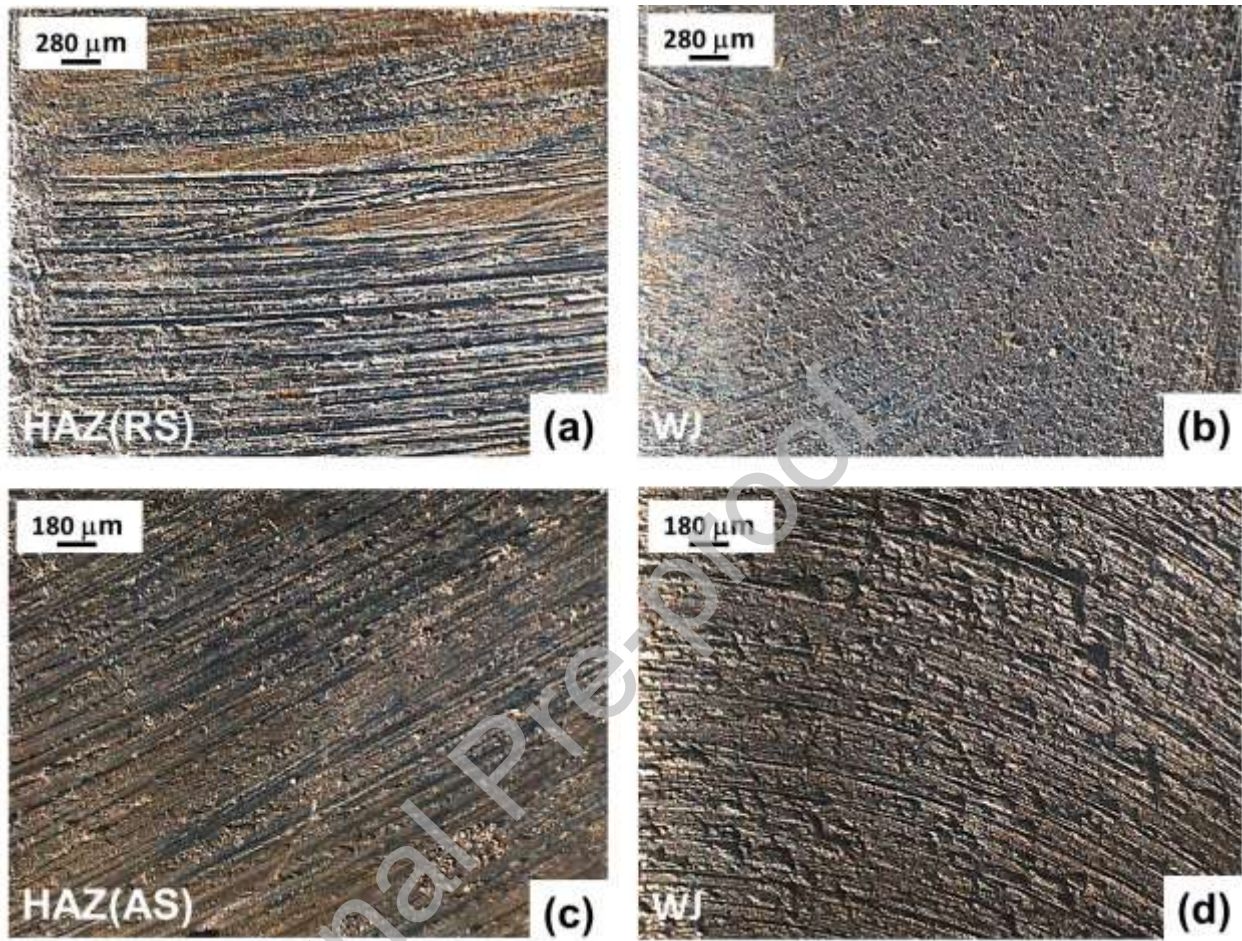


Figure 6



Declaration of interests

The authors declare that they have no known competing financial interests or personal relationships that could have appeared to influence the work reported in this paper.

The authors declare the following financial interests/personal relationships which may be considered as potential competing interests:

Journal Pre-proof

Credit authorship contribution statement

Rejane Maria P. da Silva: Conceptualization, Investigation, Data curation, Validation, Visualization, Writing – original draft, Writing – review & editing.

Javier Izquierdo: Data curation, Supervision, Visualization, Methodology, Writing – review & editing.

Mariana X. Milagre: Investigation, Writing – review & editing

João Victor de S. Araujo: Investigation, Writing – review & editing

Renato A. Antunes: Investigation, Writing – review & editing

Ricardo M. Souto: Data curation, Supervision, Methodology, Funding acquisition, Writing – original draft, Writing – review & editing.

Isolda Costa: Supervision, Resources, Funding acquisition, Writing – review & editing.